Journal Pre-proof

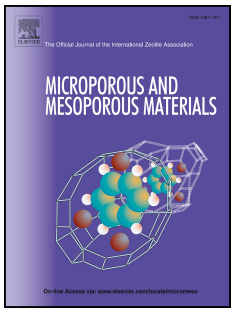

Preliminary evaluation of zeolite-based platforms as potential dual drug delivery systems against microbial infections in the tumor microenvironment

Ana Raquel Bertão, Viktoriya Ivasiv, Cristina Almeida-Aguiar, Patricia R. Correia, António M. Fonseca, Manuel Bañobre-López, Fátima Baltazar, Isabel C. Neves

PII: S1387-1811(23)00447-X

DOI: https://doi.org/10.1016/j.micromeso.2023.112871

Reference: MICMAT 112871

To appear in: *Microporous and Mesoporous Materials*

Received Date: 18 July 2023

Revised Date: 20 October 2023

Accepted Date: 24 October 2023

Please cite this article as: A.R. Bertão, V. Ivasiv, C. Almeida-Aguiar, P.R. Correia, Antó.M. Fonseca, M. Bañobre-López, Fá. Baltazar, I.C. Neves, Preliminary evaluation of zeolite-based platforms as potential dual drug delivery systems against microbial infections in the tumor microenvironment, *Microporous and Mesoporous Materials* (2023), doi: https://doi.org/10.1016/j.micromeso.2023.112871.

This is a PDF file of an article that has undergone enhancements after acceptance, such as the addition of a cover page and metadata, and formatting for readability, but it is not yet the definitive version of record. This version will undergo additional copyediting, typesetting and review before it is published in its final form, but we are providing this version to give early visibility of the article. Please note that, during the production process, errors may be discovered which could affect the content, and all legal disclaimers that apply to the journal pertain.

© 2023 Published by Elsevier Inc.

Preliminary evaluation of zeolite-based platforms as potential dual drug delivery systems against microbial infections in the tumor microenvironment

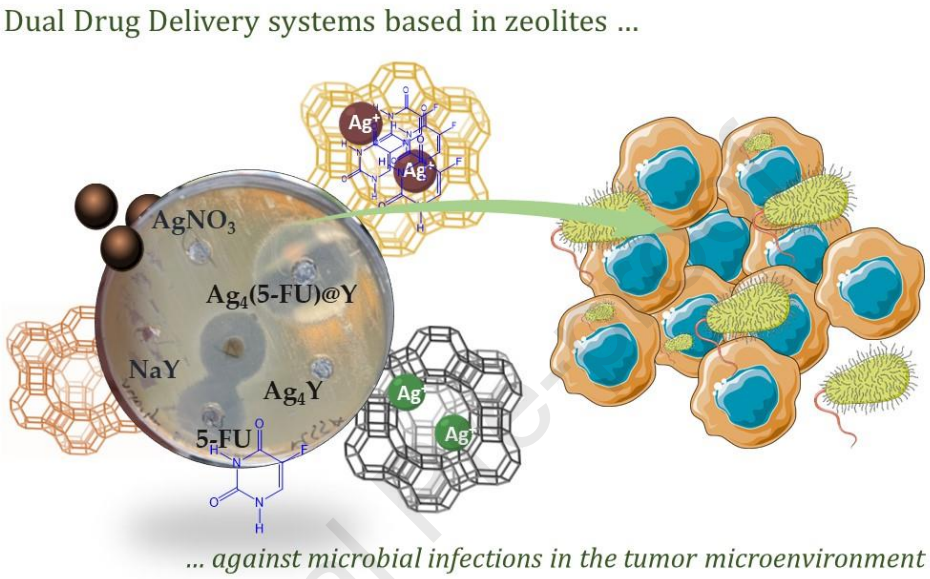

Journal Pre-proof

Preliminary evaluation of zeolite-based platforms as potential dual drug delivery systems against microbial infections in the tumor microenvironment

Ana Raquel Bertão,[a,b,c,d*] Viktoriya Ivasiv,[a] Cristina Almeida-Aguiar,[e] Patricia R. Correia,[a,e] António M. Fonseca,[a,f] Manuel Bañobre-López,[b] Fátima Baltazar,[c,d] Isabel C. Neves[a,f*]

[a]*CQUM-Centre of Chemistry, Department of Chemistry, University of Minho, Campus de Gualtar, 4710-057 Braga, Portugal;*

[b]*Advanced (magnetic) Theranostic Nanostructures Lab, Nanomedicine Group, International Iberian Nanotechnology Laboratory, Avenida Mestre José Veiga, Braga, Portugal;*

[c]*Life and Health Sciences Research Institute (ICVS), School of Medicine, University of Minho, Campus de Gualtar, Braga, Portugal;*

[d]*ICVS/3B's - PT Government Associate Laboratory, Braga/Guimarães, Portugal; FB*

[e]*CBMA - Centre of Molecular and Environmental Biology, Department of Biology, University of Minho, 4710-057 Braga, Portugal;*

[f]*CEB - Centre of Biological Engineering, University of Minho, 4710-057 Braga, Portugal.*

*Corresponding authors: ARB (id8211@alunos.uminho.pt) and ICN (ineves@quimica.uminho.pt).

Journal Pre-proof

Abstract

Several zeolite-based delivery systems (ZDS) built with *faujasite* structure were prepared containing silver (Ag^+) and 5-Fluorouracil (5-FU) as antimicrobial and antineoplastic agents, respectively. The idea behind this drug combination is an answer to the increasing evidence of colonization of tumor microenvironments by pathogenic microorganisms and their active role in tumor growth. Two ZDS with a fixed load of 5-FU and different silver loads, Ag_7(5-FU)@Y and Ag_4(5-FU)@Y, were prepared through ion-exchange of silver followed by 5-FU encapsulation in liquid phase. The developed ZDS were characterized in-depth by scanning microscopy (SEM), thermogravimetric analysis (TGA), N_2 adsorption analysis, ICP-AES analyses and X-ray photoelectron spectroscopy (XPS), and successfully confirmed the incorporation of both drug-active species into the zeolite framework without inducing structural alteration. Finally, the antimicrobial properties of the ZDS were investigated against various strains of bacteria. ZDS containing both drug-active species - Ag and 5-FU - displayed lower Minimum Inhibitory Concentration (MIC) values than Ag_xY, indicating higher effectiveness in inhibiting bacterial growth. Ag_4(5-FU)@Y resulted to be the most favourable combination exhibiting efficient encapsulation of 5-FU while containing an efficient amount of silver.

Keywords: Zeolite; 5-Fluorouracil; Silver; Microbial infections; Tumor microenvironment

1. Introduction

Antimicrobial resistance (AMR) and its impact on the health and well-being of the global population and economy has been highlighted by the World Health Organization (WHO) [1,2]. According to estimates, there were 4.95 million deaths linked to antimicrobial

resistance (AMR) in 2019, with 1.3 million directly attributed to bacterial AMR [3]. These staggering numbers motivate the creation and improvement of new and cost-effective treatment options and alternative antimicrobial solutions, while minimizing the negative impacts on human and animal health, as well as on the environment.

Bacteria play a significant role in various diseases beyond conventional bacterial infections. In the oncology field, it has been reported that bacterial infections can contribute to the development of tumor-like conditions [4-6]. One well-known example is *Helicobacter pylori*, which has been associated with gastric cancers and mucosa-associated lymphoid tissue (MALT) lymphoma [4]. This phenomenon is not limited to specific types of cancer or this bacterium, as other bacterial species have been found to have a role in cancer initiation and progression [5].

In fact, Hanahan's study [6] on cancer hallmarks identified polymorphic microbiomes as one of the "enabling characteristics" of cancer. The variability of these microbiomes amongst population individuals seems to profoundly affect cancer phenotypes [6] (Figure 1). Recent studies also suggest that malignant tumors not only exhibit specific bacterial profiles, but some of these bacteria can also compromise the efficacy of cancer therapies [7-9]. Furthermore, the immune system of cancer patients is also negatively affected, by the disease itself, or by the treatments they undergo, making them more susceptible to infections, particularly in hospital environments [10].

Journal Pre-proof

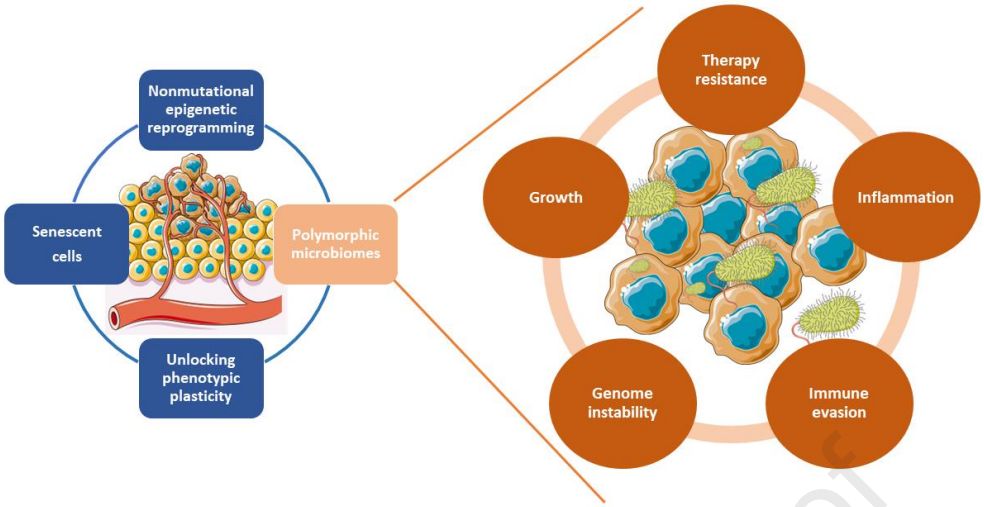

Figure 1. New "emerging hallmarks" and "enabling characteristics" of cancer, including the polymorphic microbiomes. Adapted from [6].

Therefore, the development of a treatment system that addresses two interconnected clinical scenarios: microbial infections, and potentially cancer, is highly desirable. In this context, the use of host porous structures with the capacity to accommodate multiple active species could be an interesting strategy. Zeolites, stable aluminosilicate nanomaterials, possess the unique ability to undergo an ion exchange process and effectively encapsulate other compounds within their porous structure [11]. The adsorption characteristics of zeolites rely on the capability of adsorbing molecules to enter the vacant spaces within the zeolite structures. This diffusion process is constrained by the dimensions of the molecules and the sizes of the zeolite pores. As such, zeolites have already shown the capability of stabilizing various drugs and being used as drug delivery systems [11-13].

Among the different zeolites, the *faujasite* structure stands out due to its 12-ring pore openings and three-dimensional channel system. The *faujasite* structure consists of hexagonal prisms, sodalite cages, and supercages, characterized by a low Si/Al ratio. This

unique composition allows for a high cation exchange capacity while maintaining excellent biocompatibility for health-related applications [11-18]. This framework is employed in numerous applications, including their use as adsorbents, heterogeneous catalysts, and ion-exchangers [14, 15]. With this in mind, preliminary studies were conducted as proof of concept to evaluate the capability of *faujasite*-type ZDS as a dual-host. The ion-exchange capability of zeolites was exploited in these studies, with silver being specifically chosen as one of the pharmacologically active species.

Silver is known for its antimicrobial activity [19, 20] and its antitumoral effect has also been reported against specific types of tumors [21, 22]. As reviewed by Dutta *et al.* [23], different types of zeolites have already been investigated as platforms for silver storage and delivery, either in the form of silver ions (Ag^{+}) or silver nanoparticles (AgNPs). However, to the best of our knowledge, no study has been conducted to explore the synergistic effects of silver and a chemotherapeutic drug when both are simultaneously loaded into a zeolite framework. 5-Fluorouracil (5-FU) emerges as a promising candidate for this combined approach since it is a small organic molecule, able to penetrate the micropores of a *faujasite* zeolite, as previously demonstrated in earlier studies [24, 25]. As one of the extensively utilized drugs in chemotherapy, 5-FU finds wide application in the treatment of breast, colorectal, stomach, pancreatic, and skin cancers [24, 26, 27].

Several ZDS samples were prepared by incorporating both silver and 5-FU into the NaY zeolite. The silver loading onto the zeolite framework was varied to create different samples. The resulting ZDS samples were thoroughly characterized and subsequently evaluated for their antimicrobial properties against a range of bacteria, including the Gram-negative bacteria *Escherichia coli* and *Pseudomonas aeruginosa*, as well as the Gram-positive bacteria *Staphylococcus aureus* (SA), Methicillin resistant *Staphylococcus*

aureus (MRSA), Methicillin sensitive *Staphylococcus aureus* (MSSA), *Streptococcus pyogenes* and *Propionibacterium acnes*.

By assessing their efficacy against Gram-negative and Gram-positive bacteria, we aimed to shed light on the potential applications of these dual-loaded ZDS in combating microbial infections in tumor-like microenvironments. The findings of this study have the potential to contribute to the development of novel therapeutic strategies for cancer, thereby providing enhanced treatment outcomes through a multi-angle approach.

2. Experimental

2.1 Materials and chemicals

NaY, a *faujasite*-type zeolite structure, was supplied from Zeolyst International (CBV100, Si/Al = 2.83) in powder form. Silver nitrate ($AgNO_3$) and 5-fluoro-1H, 3H-pyrimidine-2,4-dione (5-Fluorouracil, 5-FU) were provided from Fisher Scientific and Sigma Aldrich, respectively, and were used as received. Acetone (ACS reagent, ≥ 99.5%) was purchased from Sigma Aldrich, and deionized water was obtained through an ultrapure water system (Milli-Q, EQ 7000).

2.2 Preparation and characterization of the ZDS samples

To prepare the ZDS samples, a two-step process was followed: (i) Initially, the ion-exchange method described in other studies [20, 28, 29] was used to obtain two silver-NaY samples containing 4.0 and 7.0 wt% of silver (as analysed by Inductive Coupled Plasma (ICP)), named Ag_4Y and Ag_7Y, respectively. (ii) These samples were employed as hosts to encapsulate 5-FU using a previously established method [24], resulting in Ag_4(5-FU)@Y and Ag_7(5-FU)@Y. A control sample containing only 5-FU – (5-FU)@Y - was prepared in the same conditions as (ii).

To obtain ZDS samples with different silver contents, varying amounts of silver nitrate aqueous solutions (0.200 mmol/g_{NaY} or 0.400 mmol/g_{NaY}) were added to a volumetric flask. To prevent the reduction of silver ions, which are sensitive to light exposure, and undesired Ag^+ reduction reactions, the flask was coated with aluminum foil [30]. NaY was added to these silver solutions and stirred constantly at 300 rpm for 24 h, at room temperature (RT). The resulting suspensions were filtered, washed with deionized water, and dried overnight at 60 ºC. The resultant white powders were then calcined at 350 ºC for 4 h.

Before 5-FU encapsulation in the synthesized Ag_xY, the sample powders were dried at 150 ºC for 4 h, to avoid the presence of water molecules inside the pores. For the encapsulation of 5-FU, a solution of 0.577 mmol 5-FU in a solvent mixture of 80% acetone and 20% water (v/v) was added to 200 mg of the corresponding Ag_xY. The liquid-phase encapsulation process involved continuous stirring at RT for 48 h, with the system sealed to prevent solvent evaporation.

A systematic study was carried out to understand the effect of silver in the 5-FU encapsulation with the sample Ag_7(5-FU)@Y. To that purpose, the resulting suspension of Ag_7(5-FU)@Y was filtered and divided into two samples: The first one was dried in an oven at 60 ºC for 12 h, to evaporate the solvent - Ag_7(5-FU)@Y1. The second was washed after the filtration step with the same solvent used for the encapsulation of 5-FU, to eliminate any non-encapsulated 5-FU, and dried in the same conditions - Ag_7(5-FU)@Y2. The same procedure of filtration and washing was used for creating the Ag_4(5-FU)@Y sample. All the steps to obtain the final samples are schematized in Figure S1.

The samples were characterized by X-ray photoelectron spectroscopy (XPS) using a Kratos Axis-Supra instrument (Thermoscientific). Measurements were carried out using Al-Kα radiation as a monochromatic X-ray source (hν = 1486.6 eV). Photoelectrons were

collected from a take-off angle of 90º (defined as the angle between the sample surface and the axis of the XPS analyzer lens). The measurement was done in a Constant Analyzer Energy mode (CAE) with a 15 mA of emission current and 160 and 40 eV pass energy for, respectively, survey spectra and high-resolution spectra. Data analysis and atomic quantification were determined from the XPS peak areas using the ESCApe software supplied by the manufacturer Kratos Analytical.

Loading of 5-FU and thermal stability of the samples were determined by thermogravimetric analysis in an STA 409 PC Luxx® Netzsch thermal analyzer (Netzsch-Gerätebau). The atmosphere used was high-purity air (99.99 % minimum purity) with a constant flow rate of 50 cm^3/min. Crucibles of alumina oxide, supplied by Netzsch, were used as sample holders where a certain amount of sample powder was placed and heated for 65 min, between 50 and 700 ºC at a heating speed of 10 ºC/min.

Silver loading was performed by Inductively Coupled Plasma Atomic Emission Spectrometry (ICP-AES), using a Philips ICP PU 7000 Spectrometer, after acid digestion of the samples in "Laboratório de Análises" of the Instituto Superior Técnico (Portugal).

To study the morphology, SEM. Scanning electron micrographs were collected on a LEICA Cambridge S360 scanning microscope equipped with an EDX system analyzed samples. Samples were coated with a thin layer of gold under vacuum (to prevent deflection of electrons caused by particles in the air) before analysis, using a Fisons Instruments SC502 sputter coater.

The textural characterization of the samples was based on the N_2 adsorption isotherms, determined at -196 ºC with a Quantachrome NOVA 4200e apparatus. All samples were previously degassed at 150 ºC under vacuum for 1 h and then at 250 °C with a heating rate of 5 °C min^{-1} for 6 h, up to a residual pressure smaller than 0.5 Pa. The micropore volumes (V_{micro}) and mesopore surface areas (S_{meso}) were calculated by the *t*-method.

BET equation was used to calculate the surface areas. The desorption branch of the isotherm was utilized to obtain the mesoporous size distributions, using the Barrett-Joyner-Halenda (BJH) method.

2.3 Release studies

The silver release profile was studied by inductively coupled plasma-optical emission spectrometry (ICP-OES) using Optima 8000 inductively coupled plasma-optical emission spectrometer (Perkin-Elmer) [28]. The S10 Autosampler (Perkin-Elmer) was used for high throughput and automated analysis of the standard and sample solutions. For that purpose, 25 mg of the sample was added to 50 mL of a PBS buffer solution at pH 7.4 and 37 ºC for 72 h. An identical procedure used for the release assay of 5-FU was followed in this case as well. After filtration, samples were acidified with 10 µL of concentrated nitric acid 60 % (v/v) to keep metals in solution.

For *in vitro* release studies, 10 mg of the Ag_x(5-FU)@Y samples were added to 50 mL of a buffer solution of phosphate-buffered saline (PBS), simulating body fluid, with pH = 7.4 at 37 ºC. Aliquots of 5 mL of the mixture were withdrawn at predetermined intervals and replaced by the same amount of fresh buffer, to maintain the volume of released medium constant. Release studies were carried out throughout 6 h. The collected aliquots were filtered with disposable 0.20 µm nylon membrane filters. Then, the UV-vis absorption spectrum of each withdrawn sample was recorded with a UV-2501PC spectrophotometer (Shimadzu) at λ_{max} 266 nm and using PBS as a blank sample for baseline correction. Measurements were conducted in triplicate and the averaged values were considered for posterior analysis. The amount of 5-FU released was determined according to previous studies [24, 28].

2.4 Evaluation of antimicrobial activity

The Gram-negative bacteria *Escherichia coli* CECT 423 (*E. coli)* and *Pseudomonas aeruginosa* 7697099 (*P. aeruginosa),* as well as the Gram-positive bacteria Methicillin Sensitive *Staphylococcus aureus* ATCC6538 (MSSA), Methicillin Resistant *S. aureus* DB1 (MRSA) and *Propionibacterium acnes* H60803 (*Pr. acnes*) - all obtained from the culture collection of the Biology Department at the University of Minho, Pt - were used as susceptible indicator strains to evaluate the antimicrobial potential of the prepared Ag-ZDS samples. Bacterial strains were cultured in agar plates containing Lysogeny Broth medium (DifcoTM LB Broth, Sigma Aldrich) supplemented with agar 2 % (w/v) (LBA) and then incubated for 24 h at 37 ºC, to promote growth and obtain fresh cultures.

The antimicrobial action of the prepared ZDS samples as well as of the NaY zeolite precursor was evaluated through an agar dilution assay as previously described [20, 25, 28]. Different LBA media supplemented with 0.2, 0.5, 1.0, and 2.0 mg/mL of NaY, Ag_7Y, or Ag_7(5-FU)@Y2 was prepared and poured into Petri dishes. Each bacterial strain was cultured in LB at 37 ºC and 200 rpm until a mid-log growth phase was reached (OD600 ≈ 0.4 - 0.6). Then, a 5 µL drop of each culture was added (in triplicate) to the plates containing the culture medium supplemented with the above-referred ZDS samples and concentrations. In addition, a 5-FU solution at a concentration equivalent to the amount of 5-FU loaded on the (5-FU)@Y sample was also tested. After 24 h of incubation at 37 °C, the plates were examined for the presence/absence of growth. The minimum inhibitory concentration (MIC) value, defined as the lowest concentration of the sample that prevented bacterial growth, was determined for each pair of zeolite samples/bacteria tested.

Also, an agar well diffusion test was carried out with *E. coli* and *S. aureus* (MSSA and MRSA) to evaluate the bacterial growth inhibition in the presence of 0.05 mg/mL of the ZDS samples Ag_4Y, Ag_4(5-FU)@Y and NaY as well as in the presence of $AgNO_3$ (5.5

μM) and 5-FU (150 μM) solutions, used for comparison purposes. A sterile cotton swab was dipped in each bacterial inoculum, prepared as mentioned above, and then used to wipe across the surface area of an LBA plate. After that, 50 μL of each ZDS sample at 0.05 mg/mL, or of the $AgNO_3$ and 5-FU solutions, was added to the wells previously formed. A commercial disc containing the antibiotics amoxicillin/clavulanic acid (Sensi-DiskTM Amoxicillin/Clavulanic Acid 20/10 mcg, Fischer Scientific) was used as a positive control. For a negative control, two LBA plates each with bacterium and empty wells were used. After 24 h incubation at 37 °C, the plates were examined for the presence of growth inhibition zones, whose diameter was measured.

The level of significance in all the statistical analysis was set at $*p<0.05$. All assays were performed in triplicate and three independent experiments were performed. The results were expressed as mean value ± SD of the triplicate assays. Statistical analysis of the results was done using Microsoft Excel 2013® to compare antimicrobial test data sets by a 2 tailed homoscedastic Student's t-test.

3. Results and Discussion

The commercially available NaY zeolite, belonging to the *faujasite* structure family, with a Si/Al ratio of 2.83, was employed as the host material for the preparation of ZDS samples. Silver and 5-FU were selected as the pharmacologically active species to be incorporated into the zeolite framework. The preparation of the drug-loaded ZDS samples involved two steps: first, the introduction of the silver ions in the *faujasite* structure (NaY) by an ion-exchange method (1) followed by the encapsulation of 5-FU (2), as illustrated in Figure 2.

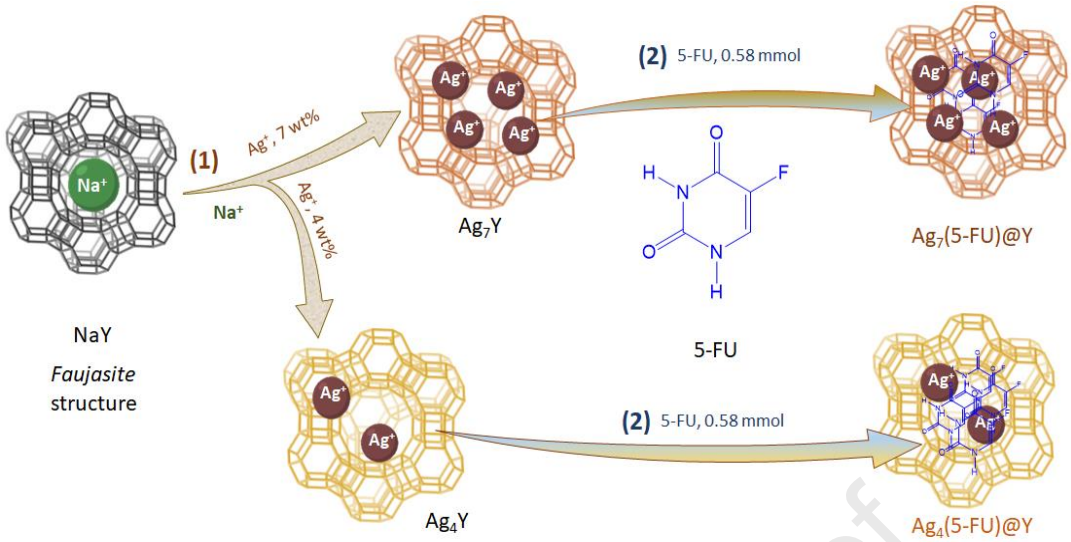

Figure 2. Two-step preparation of ZDS samples: (1) ion exchange of Ag^+ and (2) encapsulation of 5-FU.

The amount of silver in the final Ag_xY samples was quantified by ICP analysis: the Ag_7Y sample contained 7.4 wt% of silver, while Ag_4Y contained 4.2 wt% of silver. These variations in silver content are attributed to the different amounts of $AgNO_3$ utilized during the ion exchange procedure.

The N_2-physisorption isotherms of NaY, AgY, and Ag_7(5-FU)@Y are displayed in Figure S2. According to the International Union of Pure and Applied Chemistry (IUPAC) classification, AgY and Ag(5-FU)Y samples exhibit a type-I isotherm, similar to isotherm of NaY [23]. This type of isotherm is the typical pattern used to describe adsorption on microporous solid materials [16, 23]. The resemblance in the isotherms of the samples implies that the incorporation of silver ions and 5-FU into NaY has a minimal effect on the zeolite's structural characteristics [28]. The textural properties, as determined by the analysis of N_2 adsorption data, further corroborate that the introduction of silver ions and 5-FU into NaY has a minor impact on the zeolite structure (Table S1) [28].

SEM and EDX analysis of the Ag_x(5-FU)@Y zeolites highlight two aspects: (i) the experimental procedure to obtain the final samples did not affect the pristine zeolite morphology and, (ii) the presence of 5-FU at the surface (spot B) is evidenced in the sample prepared with higher amount of silver (Figure 3).

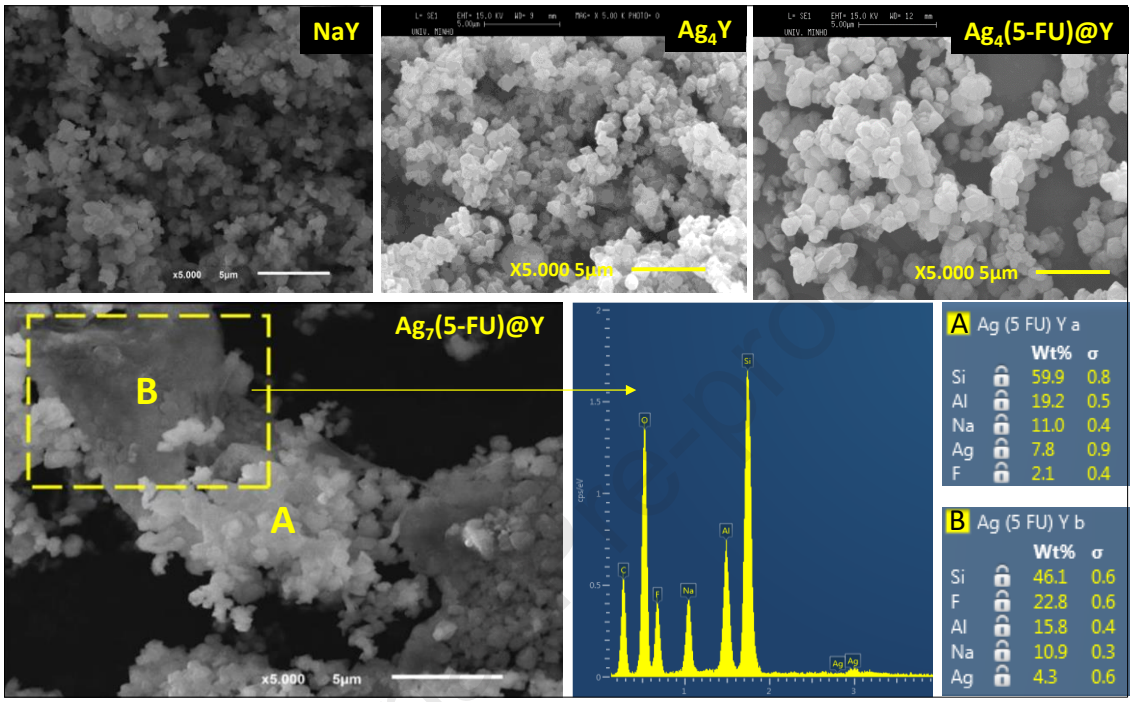

Figure 3. SEM images of NaY, Ag_4Y, Ag_4(5-FU)@Y and Ag_7(5-FU)@Y1 with 5000x magnification, and Ag_7(5-FU)@Y1 EDX spectra of the spots A and B [28].

SEM images of Ag_xY samples confirm that the NaY particles' geometry is preserved after Ag^+ incorporation through the ion-exchange method, as well as the characteristic particle size. Similarly, no morphological or structural changes were observed after the encapsulation of 5-FU to yield Ag_x(5-FU)@Y. All samples showed a typical microporous crystalline aluminosilicate structure with relatively regular small particles and well-defined geometrical shapes. The sample's average particle diameter varied from approximately 100 to 750 nm, in agreement with previous works [20, 24, 29]. This confirms that the incorporation of silver ions into the zeolite framework, as well as the

subsequent incorporation of 5-FU, had minimal impact on the size, shape, and overall morphology of the zeolite particles, which maintained their *faujasite* structure [28].

The relative weight percentage of silicon and aluminium detected by EDX further confirmed these results. The spectra revealed that the Si/Al ratios of Ag_7Y, Ag_4Y and the corresponding Ag_x(5-FU)@Y were relatively constant: 2.96 for Ag_7Y, 2.94 for Ag_4Y, 2.92 for Ag_7(5-FU)@Y1 (unwashed sample) and 2.95 for Ag_4(5-FU)@Y. These values are very close to those of the pristine NaY (2.83), meaning that the framework did not undergo significant changes during the ion exchange and subsequent 5-FU encapsulation, in agreement with N_2 adsorption analysis. Moreover, silver quantification indicated that the metal is homogeneously distributed across the Ag_7Y sample, as the amount of silver detected in different sample spots was very similar, 7.4±0.8 wt % (Figure S3). However, this was not corroborated for Ag_7(5-FU)@Y1, where more divergent amounts of silver were identified across the sample: 7.8±0.9 wt% in spot A and 4.3±0.6 wt % in spot B (Figure 3).

Regarding the 5-FU encapsulation, an important portion of 5-FU was detected at the surface of Ag_7(5-FU)@Y1 particles, although a remarkable difference was observed across the sample (22.8±0.6 wt % in the spot B whereas 2.1±0.4 wt % of 5-FU was detected in spot A). Contrary to silver atom distribution (Figure S3), the distribution of 5-FU throughout this sample was found to be highly heterogeneous. This observation suggests that the presence of silver may inhibit the accessibility of 5-FU to penetrate the zeolite structure.

XPS measurements were performed on all ZDS samples, revealing the surface composition, distribution of surface elements, and their corresponding oxidation states. The typical surface elements that predominate in all ZDS samples (O, Si, Al, and Na) were identified by the photoelectron peaks from oxygen (O 1s), silicon (Si 2p), aluminum

(Al 2s), and sodium (Na 1s) in their survey XPS spectra (Figure 4 for the samples Ag_4Y, with and without 5-FU).

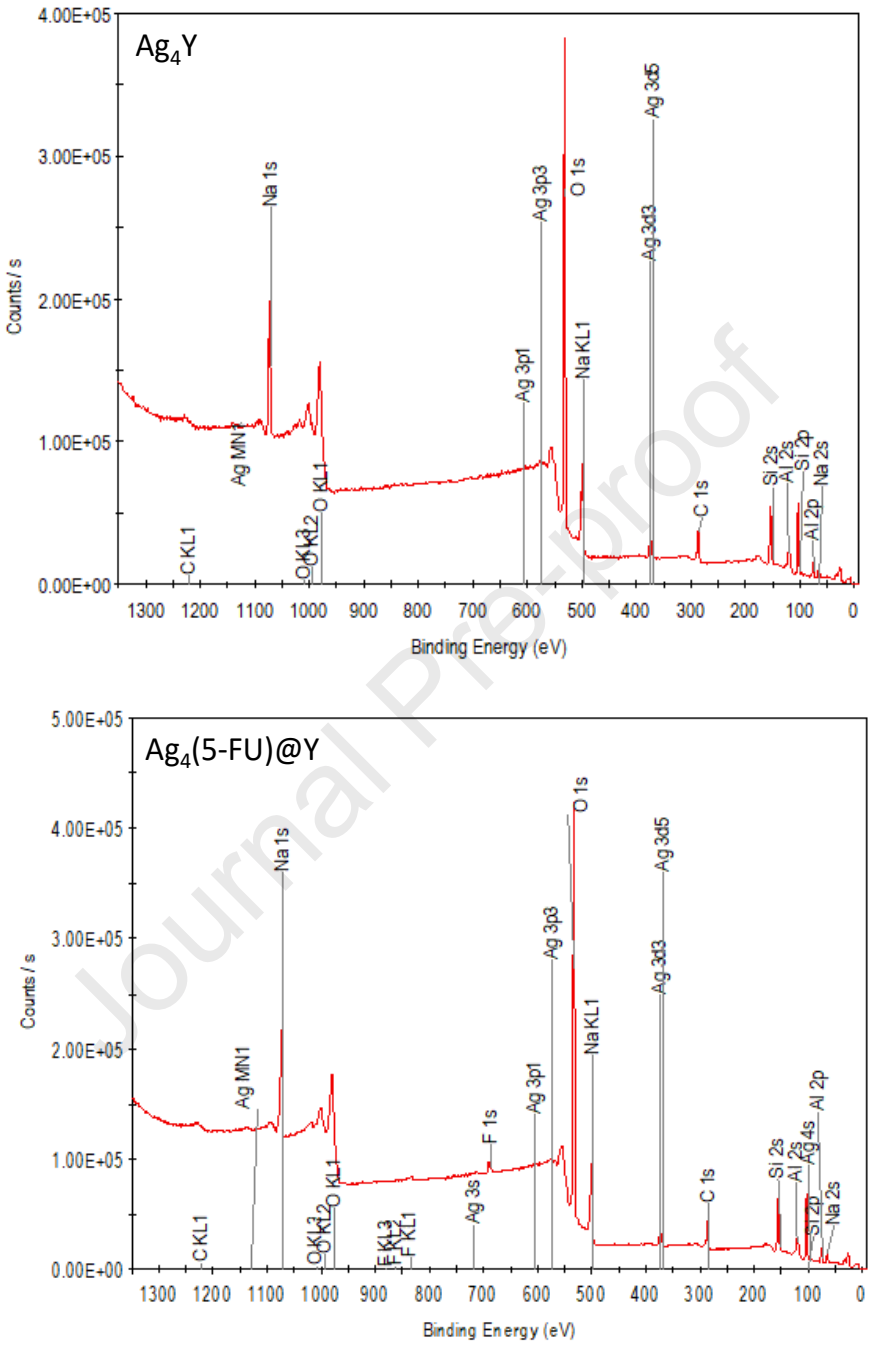

Figure 4. Survey XPS spectra of Ag_4Y and Ag_4(5-FU)@Y.

The identified O, Si, and Al atoms belonging to the zeolite are present in a distinct three-dimensional configuration, which arises from chemical bonds within the tetrahedral units

322 [SiO_4] and [AlO_4]$^-$. These units are interconnected by bridging oxygen ions, with Na^+
323 ions serving as the counter ion of the zeolite framework [29, 31]. Sodium cations (Na^+),
324 which are present in the interstice of the NaY framework to maintain the electroneutrality
325 of the structure, were progressively exchanged for Ag^+ cations during the ion exchange
326 reaction [31]. The ZDS samples with 5-FU and silver additionally displayed the presence
327 of fluorine (F 1s) and silver (Ag 3d). Table 1 illustrates the binding energies (BE) and
328 weight percentages (wt%) of the primary elements detected by XPS on the ZDS sample
329 surfaces.
330

Journal Pre-proof

331

332 **Table 1.** Binding energies (BE) and relative amount of surface elements (wt%) in the NaY and ZDS samples obtained by XPS.

XPS Peaks	Si 2p		Al 2s		Na 1s		O 1s		F 1s		Ag 3d	
	BE (eV)	wt (%)	BE (eV)	wt (%)	BE (eV)	wt (%)	BE (eV)	wt (%)	BE (eV)	wt (%)	BE (eV)	wt (%)
NaY	103.8	27.55±0.24	118.8	7.67±0.27	1074.9	10.60±0.19	534.0	54.19±0.36	-	-	-	-
Ag_7Y [28]	102.1	25.07±0.51	117.7	8.32±0.16	1072.5	8.15±0.13	532.9	54.68±0.42	-	-	368.8	3.78±0.03
Ag_4Y	102.7	27.46±0.24	117.5	7.36±0.22	1073.2	9.76±0.16	532.8	53.44±0.27	-	-	368.8	1.66±0.03
(5-FU)@Y	102.6	27.26±0.26	117.5	7.90±0.24	1072.3	7.16±0.31	532.8	53.68±0.27	689.0	0.03±0.01	-	-
Ag_7(5-FU)@Y1 [28]	103.6	28.98±0.54	117.7	8.29±0.21	1072.5	9.12±0.16	531.5	49.66±0.51	689.0	0.32±0.04	368.8	3.96±0.03
Ag_4(5-FU)@Y	102.9	30.79±0.44	117.5	10.69±0.33	1072.8	5.66±0.35	532.9	48.33±0.26	689.1	0.06±0.01	368.6	1.51±0.03

333

334

Journal Pre-proof

As shown in Table 1, the BE values of the typical zeolite elements were close to those of the NaY precursor. This confirms that the *faujasite* structure is minimally affected by the treatments employed to incorporate silver and 5-FU (namely ion-exchange and drug encapsulation), in agreement with the results from SEM/EDX analysis. For the samples subjected to the ion-exchange method, the Ag 3d photoelectron spectrum showed a single peak at approximately 369 eV indicating the presence of silver. Moreover, the amount of silver remains comparable after 5-FU encapsulation in both Ag-ZDS samples. For the sample Ag_7(5-FU)@Y1, the amount of Ag is 3.96±0.03 wt%, closer to that of Ag_7Y, 3.78±0.03 wt%. The same behaviour was observed for the ZDS samples prepared with a lower amount of silver, with 1.51±0.03 wt% and 1.66±0.03 wt% of Ag, for Ag_4(5-FU)@Y and Ag_4Y, respectively. This confirms that no lixiviation was observed after the encapsulation of the drug.

Interestingly, a discrepancy in the observed silver content is evident between the XPS and ICP results for all Ag-ZDS samples. This disparity suggests a variation in the distribution of silver within the zeolite structure: half of the total amount of silver (53.5 %) in Ag_7(5-FU)@Y1 is at the surface, while only 36.0 % of silver is detected for Ag_4(5-FU)@Y. In addition, the amount of the fluorine (F 1s) at the surface was quantified for both Ag_x(5-FU)@Y, with 0.32±0.04 wt% for Ag_7(5-FU)@Y1 and 0.06±0.01 wt% for Ag_4(5-FU)@Y, which corresponds to 0.170 mmol and 0.032 mmol, respectively. These values seem to indicate that higher amounts of 5-FU are present on the surface of Ag_7(5-FU)@Y1, compared to Ag_4(5-FU)@Y. This discrepancy in the F relative amounts between the Ag_x(5-FU)@Y samples can be attributed to the more limited diffusion of 5-FU into the zeolite structure when a higher amount of silver is encapsulated, in accordance with the SEM/EDX results.

The deconvolution of the F 1s core level shows the presence of three peaks at BE of 689.6, 691.2, and 693.3 eV for Ag_7(5-FU)@Y, and two peaks at 686.1 and 689.5 eV for Ag_4(5-FU)@Y, respectively. The peak closer to 689.0 eV for the fluorine atoms confirms the presence of the drug in both Ag-ZDS. These results are in good agreement with values reported in the literature for 5-FU and confirm the molecular integrity of the molecule [31-33].

Besides allowing the identification and quantification of surface elements in the sample, XPS also provides valuable information regarding the oxidation state of these elements. In the case of Ag-ZDS samples, the high-resolution spectra of the Ag 3d core level in the samples underwent peak deconvolution, enabling the recognition of separate peaks that originated from photoelectrons in the Ag 3d orbitals. This process also facilitated the determination of the associated binding energy values. In all the Ag-ZDS samples, two main peaks corresponding to Ag $3d_{5/2}$ and Ag $3d_{3/2}$ regions were detected at 368.8 eV and 374.6 eV, respectively. These BE values remain unaltered after the encapsulation of 5-FU (see Figure 5 for Ag 3d high resolution and kinetic spectra of the representative Ag_7Y and Ag_7(5-FU)@Y1 samples) and suggested the presence of silver in its ionic Ag^+ form [29, 34], which acts as counter-ion of the negative framework.

Journal Pre-proof

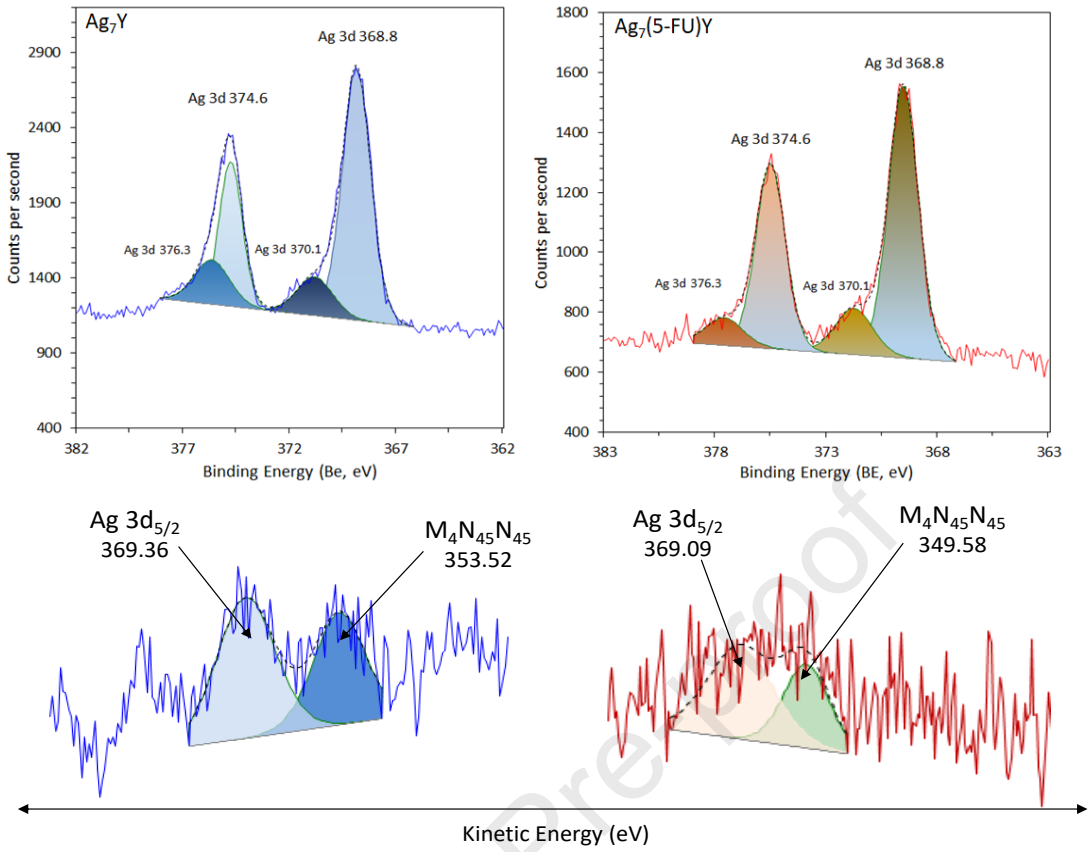

Figure 5. The deconvolution of Ag 3d high-resolution and kinetic spectra of Ag_7Y and Ag_7(5-FU)@Y1 (B) [28].

To confirm the oxidation state of silver in all Ag-ZDS samples, the Auger parameter was calculated using the equation: BE (Ag $3d_{5/2}$) + KE (Ag M_4NN), where BE represents the binding energy of photoelectron peak for Ag $3d_{5/2}$, and KE is the Auger kinetic energy [35]. The calculated Auger parameter values were 722.9 eV for Ag_7Y and 717.0 eV for Ag_4Y. For Ag_x(5-FU)@Y, the Auger parameter values were found to be 718.7 eV and 716.8 eV for Ag_7(5-FU)@Y1 and Ag_4(5-FU)@Y, respectively. These results are similar among the Ag-ZDS samples and are in good agreement with the Auger parameter values reported for the ionic state of silver (Ag^+) [36, 37].

The release of silver was representatively studied in the Ag_7(5-FU)@Y2 sample by ICP-OES, given the higher amount of silver in this sample compared to Ag_4(5-FU)@Y [28],

thus maximizing detection capability. The release was performed in a phosphate buffer solution (PBS) at a pH of 7.4 and 37 ºC simulating body fluid conditions, for a period of 72 h (Figure 6).

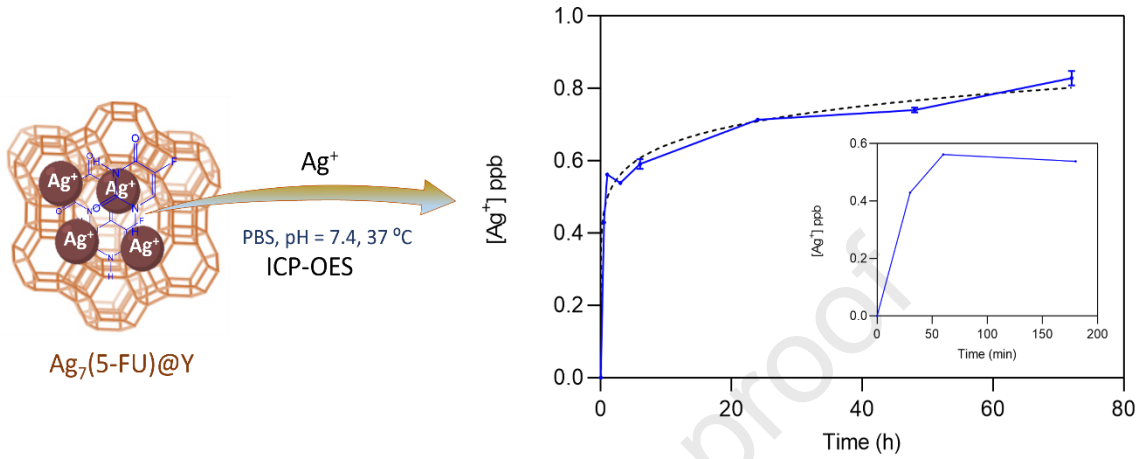

Figure 6. Release profiles of Ag+ ions from Ag7(5-FU)@Y2 (blue curve) determined by ICP-OES, and the tendency profile. Measurements were conducted in simulated physiological conditions, using a PBS solution at pH=7.4 and 37 ºC [28]. The results are expressed as the mean Ag^+ concentration ± SD of three independent assays performed in triplicate.

Notably, the ZDS released very small amounts of silver with an initial burst observed during the initial 6-hour period. Subsequently, a gradual and sustained release was observed over time throughout the whole experiment. At the end of the experiment, only $8.28x10^{-4}$ ppm of silver was released, which accounts for less than 1% of the initial silver amount (7.4 wt%). The electrostatic forces inherent to the zeolite structure play a crucial role in stabilizing the silver as a counter-ion within its negative framework. The minimal release is very likely due to the depletion of silver species on the outer surface, provoking the migration of a part of the stored silver within the structure to the surface to continue its action.

Thermogravimetric analysis (TGA) was conducted to assess the loading of 5-FU in Ag-ZDS samples over a temperature range of 50-700 ºC (Figure S4). All the samples exhibited similar behaviour up to about 150 ºC, with a weight loss associated with the removal of physisorbed water in the zeolite structure. An additional extended weight loss was observed from 430 to 600 ºC, ascribed to the melting of the 5-FU and its subsequent degradation [24, 32]. Table 2 displays the TGA results for the Ag_xY samples loaded with 5-FU. The ZDS samples containing silver present a lower efficiency for the encapsulation of 5-FU when compared to the NaY precursor (0.460 mmol of 5-FU).

Table 2. Loading of 5-FU in the ZDS samples.

ZDS	R_{Theo}[1]	R_{Exp}[1,2]	5-FU (mmol/g_{NaY})[2]
5-FU@Y	0.375	0.299	2.30
Ag_7(5-FU)@Y1 [28]	0.375	0.144	1.15
Ag_4(5-FU)@Y	0.375	0.190	1.46

[1] R_{Theo} and R_{Exp} are the theoretical and experimental ratios, respectively, of [5-FU]/NaY (wt/wt); [2] 5-FU loading in NaY determined by TGA.

The ion-exchange of silver in solution occurs between two univalent cations, Na^+ and Ag^+, described by the following reaction:

$$NaY + Ag^+ (aq) \leftrightarrow AgY + Na^+ (aq).$$

The exchange occurs between both cations and, as a result, the Ag^+ ions will occupy the different crystallographic sites of the *faujasite* structure [33, 34]. The ionic radius of Na^+ is 0.95 Å while Ag^+ is 1.14 Å [29]. Replacing Na^+ with Ag^+ led to a 1.2-fold increase in the ionic radius. Consequently, the crystallographic sites occupied by Ag^+ ions imposed certain limitations on the diffusion of 5-FU into the structure. This effect was particularly

pronounced in the case of Ag_7(5-FU)@Y. For this sample, the 5-FU loading was 0.223 mmol and 0.170 mmol for Ag_7(5-FU)@Y1 (unwashed) and Ag_7(5-FU)@Y2 (washed) samples, respectively. According to the amount of 5-FU at the surface detected by XPS for the unwashed sample, these results point out that only 25% of 5-FU was inside the structure. As the amount of silver is reduced, such as in Ag_4(5-FU)@Y, the amount of 5-FU inside the structure increases (0.260 mmol), in good agreement with the values obtained from TGA (0.292 mmol) and XPS (0.032 mmol at the surface).

To confirm this evidence, the cumulative release behaviour of 5-FU from unwashed and washed samples [28] of Ag_7(5-FU)@Y_x, was monitored for 6 h, in a PBS solution at pH 7.4, by UV/vis spectrophotometry (Figure 7). The concentration of 5-FU released was measured over time at 266 nm, the characteristic wavelength of the maximum absorption peak of 5-FU.

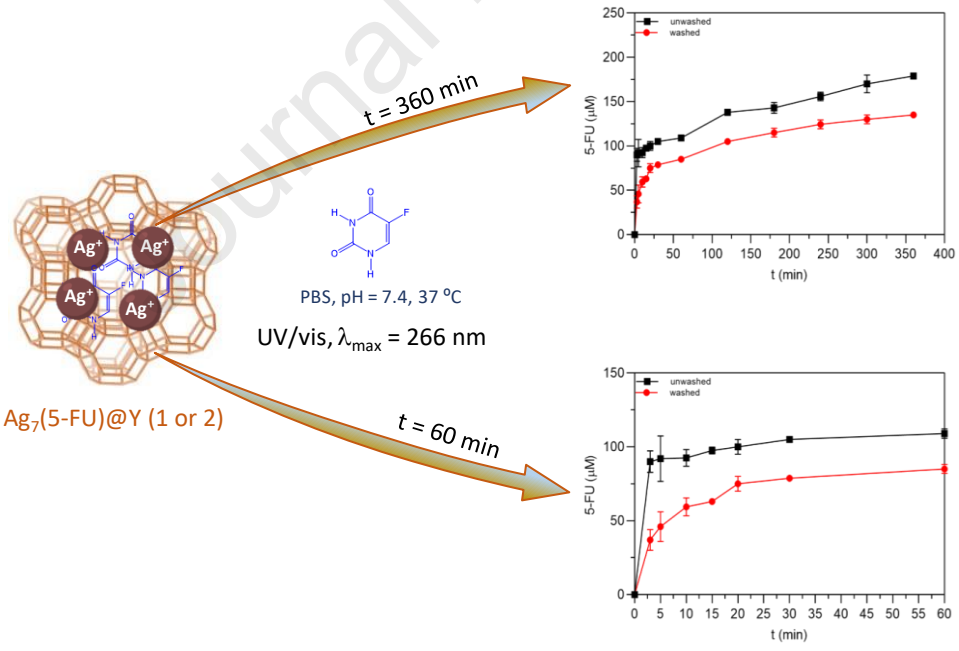

Figure 7. Release profiles of 5-FU from Ag_7(5-FU)@Y samples as determined by UV/vis during 6 h and 1 h. Measurements were conducted in simulated physiological conditions in triplicate, using a phosphate buffer solution (PBS) at pH=7.4 and 37 ºC [28]. The results

are expressed as the mean 5-FU concentration ± SD of three independent assays performed in triplicate.

The results indicate that after 5-FU release from Ag_7(5-FU)@Y_x samples, the compound showed a similar characteristic wavelength of its maximum absorption, thereby confirming its molecular integrity after encapsulation (Figure S5). The 5-FU release profile for the unwashed and washed Ag_7(5-FU)@Y_x samples was similar between them. Both profiles presented an initial burst release followed by a steady regime in which the cumulative 5-FU concentration stabilized after 30 min and increased continuously over time until the end of the assay (6 h).

However, in the washed sample, the release of the drug was slightly different with a steeper initial slope in the beginning followed by the same behaviour as the unwashed sample. During the initial 15 min, approximately 50% of the 5-FU was released from the Ag_7(5-FU)@Y1 sample, while the Ag_7(5-FU)@Y2 sample exhibited a slightly lower release (35%). This means that from 30 min onwards, the diffusion of 5-FU depends on the structure of the host, as is evident from the release profiles present in Figure 7. The desorption of 5-FU from both Ag_7(5-FU)@Y samples at 1 h was consistent with previous studies [24, 26, 32], and the diffusion of 5-FU, attributed to its small organic molecular size, is controlled by the limitations imposed by the Ag^+ ions [24].

The difference in drug release between the two cases is likely due to the different amounts of 5-FU adsorbed on the zeolite's surface, which in the washed sample was effectively removed by the solvent during the washing step. Mathematical kinetic models usually used to describe *in vitro* drug dissolution and release from pharmaceutical dosage formulations [38] can also represent these behaviours. Table S2 summarizes the selected release kinetic models used for the coefficient of determination (R^2) which indicates the

best-fit model for each sample. The zero-order model provides a better description of the release pattern observed in the unwashed sample, Ag_7(5-FU)@Y1, as evidenced by its equation displaying the highest level of linearity (Zero-order, R^2 = 0.9781). In broad agreement with previous studies [16, 24, 25] using the same host, the Weibull model (R^2 = 0.9846) is the best for the washed sample, Ag_7(5-FU)@Y2.

In summary, the characterization results indicate that high silver concentrations pre-loaded within the zeolite framework hinder 5-FU accessibility into the zeolite structure. On the other hand, lower silver concentrations seem to have a minor effect on the diffusion of 5-FU into the zeolite's structure. Consequently, higher 5-FU levels on the zeolite surface, attributed to a higher silver content, result in reduced drug loading in contrast with the ZDS with a lower amount of silver.

3.1 Antimicrobial activity assays

The antimicrobial activity of the prepared Ag-ZDS samples was evaluated against the Gram-negative bacteria *E. coli* and *P. aeruginosa*, as well as the Gram-positive bacteria Methicillin Sensitive *S. aureus* (MSSA), Methicillin Resistant *S. aureus* (MRSA) and *Pr. acnes*. These bacterial species, selected as susceptible indicator strains, are known for their capacity to cause infections [36-39] and have been recently associated with different types of malignant tumors. Indeed, *E. coli* has been directly associated with the promotion of colorectal cancer [40]. In addition, it has been already shown that this bacterium has the potential to inhibit the activity of several chemotherapeutic drugs [5, 6]. Skin wounds also create a favourable and nutrient-rich environment for the growth of bacteria such as *E. coli* and *P. aeruginosa*. These flagellated bacteria seem to have tumor-promoting effects on wound-induced skin cancer [41]. Also correlated with the progression of skin cancer is an overabundance of *S. aureus*, with a role in tumor growth already described

in the literature [42]. Furthermore, the potential involvement of *Pr. acnes* in the carcinogenesis of prostate and ovarian cancers was also reported [43, 44].

First, the antibacterial activity of the ZDS samples with higher amounts of silver was assessed by testing increasing concentrations of the samples (0.2, 0.5, 1.0, and 2.0 mg/mL) and determining the respective MIC values against the chosen bacterial panel by an agar dilution test (Figure 8 and Table 3).

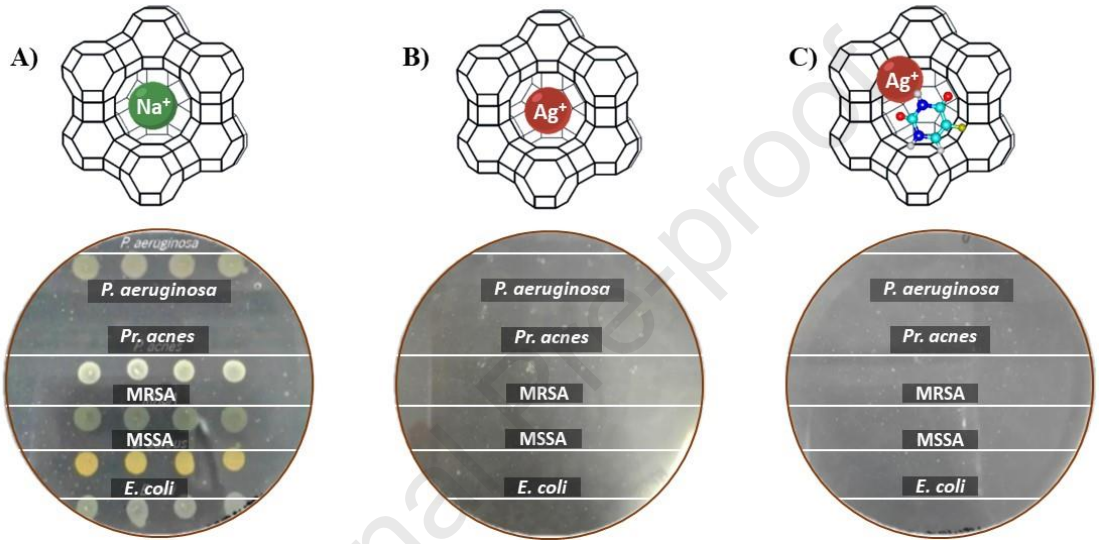

Figure 8. Antimicrobial potential of 2.0 mg/mL NaY (A), 1.0 mg/mL Ag_7Y (B), and 0.5 mg/mL Ag_7(5-FU)@Y2 (C). Images show the presence/absence of growth of *P. aeruginosa*, *Pr. acnes*, MRSA, MSSA, and *E. coli* in an LBA medium supplemented with the referred ZDS-samples and concentrations [28].

Table 3 summarizes the results obtained in agar dilution tests for the samples against the microorganisms studied.

Table 3. MIC values (mg/mL) for the samples tested against the chosen panel of microorganisms [28].

Journal Pre-proof

Microorganisms	NaY	Ag_7Y	Ag_7(5-FU)@Y2
Pr. acnes	>2	0.5	0.5
MRSA	>2	1.0	0.5
MSSA	>2	1.0	0.2
E. coli	>2	0.5	0.5
P. aeruginosa	>2	1.0	0.5

The analysis of results shows that every strain grew equally in the presence of NaY, regardless of the concentration of the system tested, meaning that the zeolite itself has no antibacterial effect. This was an expected result since precursor zeolites have been described as inert and devoid of antimicrobial properties [20, 29].

On the other hand, Ag_7Y exhibited antibacterial activity against all tested strains, and no bacterial growth was detected in the presence of 1.0 mg/ mL (Figure 8), or even 0.5 mg/mL, depending on the strain (Table 3). Ag_4Y has also shown a MIC of 0.5 mg/mL for *E. coli* as described in previous work [29]. The introduction of silver in its ionic state into the zeolite framework seems to provide the material with antibacterial properties.

Interestingly, Ag_7(5-FU)@Y2 has lower MIC values than Ag_7Y when tested against MRSA, MSSA, and *P. aeruginosa* (Table 3), suggesting that 5-FU might also exert an antimicrobial effect together with the silver ions on the zeolite. In fact, although it is widely known as a cytotoxic agent for cancer cells, 5-FU was reported to exhibit inhibitory effects on the growth and viability of several microorganisms [45, 46]. According to the literature, the first study of the antimicrobial action of 5-FU was performed in *E. coli* and showed that its inhibitory effects resulted from the intracellular conversion of 5-FU to the metabolite fluorodeoxyuridylate (FdUMP). Thymidine starvation causes the cessation of DNA synthesis and repair and finally ends in the so-

called ‘thymineless death’ [45]. Another study suggested the perturbation of the cell wall biosynthesis as a mechanism of 5-FU toxicity towards *E. coli*. It was demonstrated that 5-FU partially inhibited the synthesis of the cell wall mucopeptide in *S. aureus* (MSSA) [46]. In a study exploring the antibacterial activity of antineoplastic agents, 5-FU was one of the few antineoplastic agents with appreciable inhibitory effects, showing activity against > 80% of the bacterial isolates tested [47].

To understand the effect of 5-FU in all strains, a control with 5-FU at a concentration equivalent to the one present in Ag_7(5-FU)@Y2 was studied. Figure 9 shows that the outcome of 5-FU treatment was not homogeneous in all strains. For example, the viability of *P. aeruginosa* and MRSA was not affected, as both strains grew equally in the absence (control) and the presence of 5-FU in the culture medium. The 5-FU concentration used in these cases seems to have no effect, contrary to what was described in the literature [45-47], but that could also be explained by the different characteristics of the used strains.

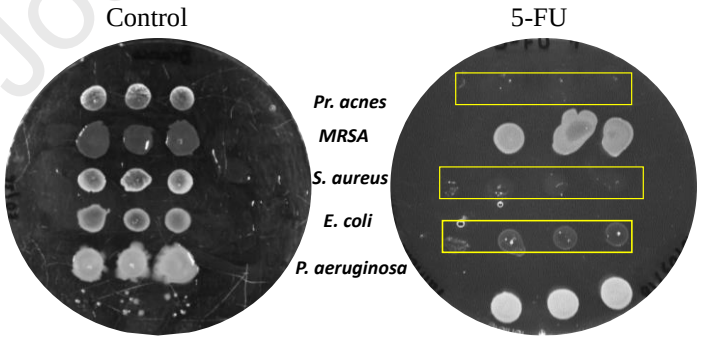

Figure 9. Antimicrobial activity assays in the absence and presence of 5-FU solution corresponding to the 5-FU concentration present in 0.5 mg/mL of ZDS [28], after 24 h of incubation.

According to these results, the lower MIC values observed for Ag_7(5-FU)@Y against *P. aeruginosa* and *S. aureus*, both MRSA and MSSA (Table 3), cannot be justified by either the presence of 5-FU (Figure 9) or Ag alone within the range of concentrations tested. The results suggest a synergistic effect coming from the combination of 5-FU with the strong microbicidal capabilities of silver ions, which effectively suppress bacterial growth. In the case of *S. aureus*, no growth was observed when exposed to 5-FU alone (Figure 9). These findings may account for the notable difference in the MIC values between Ag_7Y and Ag_7(5-FU)@Y, as indicated in Table 3. Specifically, the MIC value was lower after the loading of 5-FU in the ZDS sample, suggesting that the incorporation of 5-FU resulted in an increased antimicrobial activity. Regarding *E. coli*, the bacterium only grew slightly in the presence of 5-FU, which highlights the inhibitory properties of 5-FU against *E. coli*, but suggests that this concentration is still insufficient to completely abolish bacterial growth.

As Ag-ZDS samples with a lower amount of silver allow more effective 5-FU encapsulation, the performance of Ag_4Y and Ag_4(5-FU)@Y, along with NaY and (5-FU)@Y was assessed. This comparison was conducted through agar well diffusion tests using *E. coli* and *S. aureus* (MSSA and MRSA) as susceptible indicator strains. In this case, a lower concentration of the system was used in the test (0.05 mg/mL), as this concentration ensured optimal cell cytotoxicity without compromising nutrient exchange in cancer cell assays [48].

A similar effect of 5-FU antibacterial activity was observed in the agar well diffusion test for MRSA, MSSA, and *E. coli*, suggesting that 5-FU might also exert an antimicrobial effect together with the silver ions (data not shown). The results indicate that only MSSA exhibits inhibition when exposed to (5-FU)@Y and Ag_4(5-FU)@Y. For samples with lower Ag content, such as Ag_4Y and Ag_4(5-FU)@Y, growth inhibition was observed for

the sample loaded with 5-FU, whereas the other bacteria showed no inhibition in the presence of NaY, Ag_4Y, (5-FU)@Y, and Ag_4(5-FU)@Y (data not shown). In addition, the inhibition halo of Ag_4(5-FU)@Y seems to increase in dimension compared to 5-FU alone (Figure 10), with the following distribution: Ag_4(5-FU)@Y > 5-FU > antibiotic.

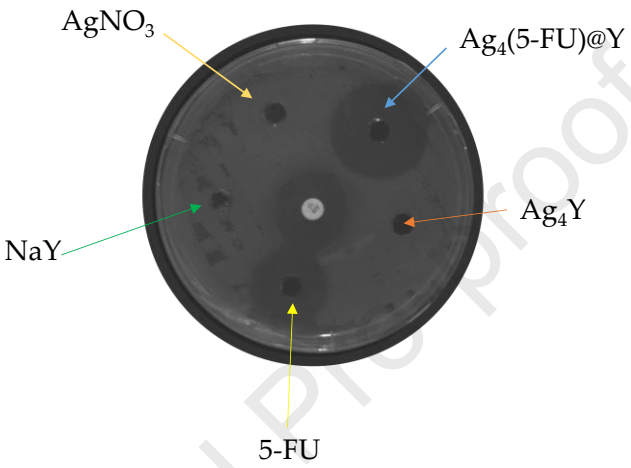

Figure 10. Antimicrobial activity assay with NaY, $AgNO_3$, Ag_4Y, Ag_4(5-FU)@Y, and 5-FU solution against MSSA, after 24 h of incubation using agar well diffusion test.

Interestingly, these results suggest that, in the dual system, the combined effect of both 5-FU and Ag^+ is possibly contributing to the antimicrobial activity of this ZDS. To the best of our knowledge, the use of silver-loaded zeolites together with pharmaceutical agents has been primarily documented in the context of their combination with antibiotics. For instance, the simultaneous release of the antibiotic sulfadiazine and the silver ions using a zeolite beta framework exhibited enhanced efficacy against a range of microorganisms [49]. In another study, the silver-loaded *faujasite* zeolite, Ag-Z, enhanced the effectiveness of rifampicin against *E. coli* [50]. Due to the drugs under investigation and the different methods employed, conducting a direct comparison with

our study may not be feasible. Nevertheless, the results highlight the potential role played by silver-supported zeolites in achieving improved antibacterial efficacy.

Although both Ag-loaded ZDS samples showed promising results, a reduced level of silver will always be advantageous for ZDS in anticancer applications. The characterization results of Ag_4(5-FU)@Y further revealed a more uniform distribution of 5-FU within the zeolite framework, along with an increased drug loading. To further enhance the antineoplastic efficacy of these samples, future studies could explore the combined effects of 5-FU@Y with Ag_4Y or 5-FU@Y with Ag_4(5-FU)@Y. Such an approach holds promise for improving the anticancer properties of these samples and contributes to their potential as effective delivery systems with dual properties, including antimicrobial and antitumor activities. Indeed, the development of dual-action nanoparticles, based on liposomes, has already demonstrated promising results in addressing cancer-related bacterial infections, with improved cytotoxicity outcomes [51]. However, it is worth emphasizing that the use of zeolites in this context has been relatively overlooked but seems to have the potential to serve as efficient and cost-effective alternatives.

4. Conclusions

In conclusion, this study focused on the development of zeolite-based delivery systems (ZDS) using a *faujasite* structure and incorporating silver (Ag^+) and 5-Fluorouracil (5-FU) as antimicrobial and antineoplastic agents, respectively. Two ZDS samples, Ag_7(5-FU)@Y and Ag_4(5-FU)@Y, were prepared by varying the initial silver nitrate amounts using an ion-exchanged method. The characterization analysis confirmed the successful incorporation of both species without significant changes to the zeolite structure. Both SEM/EDX and XPS results revealed that the presence of silver within the framework hindered the diffusion of 5-FU, particularly in the case of Ag_7(5-FU)@Y_x. This leads to

higher amounts of 5-FU on the zeolite surface and consequently to a lower drug loading when compared to the ZDS with less amount of silver. Finally, the results of antimicrobial assays indicate that the antimicrobial activity of the ZDS may be attributed to the combined effect of both 5-FU and Ag^+ in the dual system. However, Ag_4(5-FU)@Y might represent the best compromise between effective 5-FU loading, optimal silver content, and antibacterial activity. These findings suggest that the combined effects of 5-FU@Y and Ag_4Y or 5-FU@Y and Ag_4(5-FU)@Y could hold significant potential for enhancing the antineoplastic properties of these samples, thus contributing to their application in cancer therapy.

Conflicts of interest

There are no conflicts of interest to declare.

Acknowledgments

A.R.B. and V.I. thank to Foundation for Science and Technology (FCT, Portugal) for their Ph.D. grants (SFRH/BD/141058/ 2018 and UI/BD/152219/2021, respectively). This research work has been funded by national funds funded through FCT/MCTES (PIDDAC) over the projects: project UIDB/50026/2020 and UIDP/50026/2020, the project NORTE-01-0145-FEDER-000055, Centre of Chemistry (UID/QUI/0686/2020), CEB (UIDB/04469/2020), and UIDP/50026/2020 (ICVS). Additionally, the projects of BioTecNorte (operation NORTE-01-0145-FEDER-000004 and NORTE-01-0145-FEDER-000055), supported by the Norte Portugal Regional Operational Program (NORTE 2020), under the PORTUGAL 2020 Partnership Agreement, through the European Regional Development Fund (ERDF). This work was also supported by the "Contrato-Programa" UIDB/04050/2020 funded by national funds through the FCT I.P.

The authors thank Doctor O.S.G.P. Soares (University of Porto, Portugal) for the N_2 adsorption analysis.

References

[1] World Health Organization, Ten threats to global health in 2019. https://www.who.int/news-room/spotlight/ten-threats-to-global-health-in-2019, 2019 (accessed May 30, 2023).

[2] E. Tacconelli, E. Carrara, A. Savoldi, S. Harbarth, M. Mendelson, D.L. Monnet, C. Pulcini, G. Kahlmeter, J. Kluytmans, Y. Carmeli, M. Ouellette, K. Outterson, J. Patel, M. Cavaleri, E.M. Cox, C.R. Houchens, M.L. Grayson, P. Hansen, N. Singh, U. Theuretzbacher, N. Magrini, A.O. Aboderin, S.S. Al-Abri, N. Awang Jalil, N. Benzonana, S. Bhattacharya, A.J. Brink, F.R. Burkert, O. Cars, G. Cornaglia, O.J. Dyar, A.W. Friedrich, A.C. Gales, S. Gandra, C.G. Giske, D.A. Goff, H. Goossens, T. Gottlieb, M. Guzman Blanco, W. Hryniewicz, D. Kattula, T. Jinks, S.S. Kanj, L. Kerr, M.-P. Kieny, Y.S. Kim, R.S. Kozlov, J. Labarca, R. Laxminarayan, K. Leder, L. Leibovici, G. Levy-Hara, J. Littman, S. Malhotra-Kumar, V. Manchanda, L. Moja, B. Ndoye, A. Pan, D.L. Paterson, M. Paul, H. Qiu, P. Ramon-Pardo, J. Rodríguez-Baño, M. Sanguinetti, S. Sengupta, M. Sharland, M. Si-Mehand, L.L. Silver, W. Song, M. Steinbakk, J. Thomsen, G.E. Thwaites, J.W.M. van der Meer, N. Van Kinh, S. Vega, M.V. Villegas, A. Wechsler-Fördös, H.F.L. Wertheim, E. Wesangula, N. Woodford, F.O. Yilmaz, A. Zorzet, Lancet Infect. Dis. 18 (2018) 318–327. https://doi.org/10.1016/S1473-3099(17)30753-3

[3] C.J.L. Murray, K.S. Ikuta, F. Sharara, L. Swetschinski, G. Robles Aguilar, A. Gray, C. Han, C. Bisignano, P. Rao, E. Wool, S.C. Johnson, A.J. Browne, M.G. Chipeta, F. Fell, S. Hackett, G. Haines-Woodhouse, B.H. Kashef Hamadani, E.A.P. Kumaran, B. McManigal, S. Achalapong, R. Agarwal, S. Akech, S. Albertson, J. Amuasi, J. Andrews, A. Aravkin, E. Ashley, F.-X. Babin, F. Bailey, S. Baker, B. Basnyat, A. Bekker, R. Bender, J.A. Berkley, A. Bethou, J. Bielicki, S. Boonkasidecha, J. Bukosia, C. Carvalheiro, C. Castañeda-Orjuela, V. Chansamouth, S. Chaurasia, S. Chiurchiù, F. Chowdhury, R. Clotaire Donatien, A.J. Cook, B. Cooper, T.R. Cressey, E. Criollo-Mora, M. Cunningham, S. Darboe, N.P.J. Day, M. De Luca, K. Dokova, A. Dramowski, S.J. Dunachie, T. Duong Bich, T. Eckmanns, D. Eibach, A. Emami, N.

Feasey, N. Fisher-Pearson, K. Forrest, C. Garcia, D. Garrett, P. Gastmeier, A.Z. Giref, R.C. Greer, V. Gupta, S. Haller, A. Haselbeck, S.I. Hay, M. Holm, S. Hopkins, Y. Hsia, K.C. Iregbu, J. Jacobs, D. Jarovsky, F. Javanmardi, A.W.J. Jenney, M. Khorana, S. Khusuwan, N. Kissoon, E. Kobeissi, T. Kostyanev, F. Krapp, R. Krumkamp, A. Kumar, H.H. Kyu, C. Lim, K. Lim, D. Limmathurotsakul, M.J. Loftus, M. Lunn, J. Ma, A. Manoharan, F. Marks, J. May, M. Mayxay, N. Mturi, T. Munera-Huertas, P. Musicha, L.A. Musila, M.M. Mussi-Pinhata, R.N. Naidu, T. Nakamura, R. Nanavati, S. Nangia, P. Newton, C. Ngoun, A. Novotney, D. Nwakanma, C.W. Obiero, T.J. Ochoa, A. Olivas-Martinez, P. Olliaro, E. Ooko, E. Ortiz-Brizuela, P. Ounchanum, G.D. Pak, J.L. Paredes, A.Y. Peleg, C. Perrone, T. Phe, K. Phommasone, N. Plakkal, A. Ponce-de-Leon, M. Raad, T. Ramdin, S. Rattanavong, A. Riddell, T. Roberts, J.V. Robotham, A. Roca, V.D. Rosenthal, K.E. Rudd, N. Russell, H.S. Sader, W. Saengchan, J. Schnall, J.A.G. Scott, S. Seekaew, M. Sharland, M. Shivamallappa, J. Sifuentes-Osornio, A.J. Simpson, N. Steenkeste, A.J. Stewardson, T. Stoeva, N. Tasak, A. Thaiprakong, G. Thwaites, C. Tigoi, C. Turner, P. Turner, H.R. van Doorn, S. Velaphi, A. Vongpradith, M. Vongsouvath, H. Vu, T. Walsh, J.L. Walson, S. Waner, T. Wangrangsimakul, P. Wannapinij, T. Wozniak, T.E.M.W. Young Sharma, K.C. Yu, P. Zheng, B. Sartorius, A.D. Lopez, A. Stergachis, C. Moore, C. Dolecek, M. Naghavi, Lancet. 399 (2022) 629–655. https://doi.org/10.1016/S0140-6736(21)02724-0

[4] L.E. Wroblewski, R.M.J. Peek, K.T. Wilson, Clin. Microbiol. Rev. 23 (2010) 713–739. https://doi.org/10.1128/cmr.00011-10

[5] A. Basu, R. Singh, S. Gupta, Wiley Interdiscip. Rev. Nanomedicine Nanobiotechnology. 14 (2022) e1771. https://doi.org/10.1002/wnan.1771

[6] D. Hanahan, Cancer Discov. 12 (2022) 31–46. https://doi.org/10.1158/2159-8290.CD-21-1059

[7] G.D. Sepich-Poore, L. Zitvogel, R. Straussman, J. Hasty, J.A. Wargo, R. Knight, Science (80-.). 371 (2021) eabc4552. https://doi.org/10.1126/science.abc4552

[8] L.T. Geller, M. Barzily-Rokni, T. Danino, O.H. Jonas, N. Shental, D. Nejman, N. Gavert, Y. Zwang, Z.A. Cooper, K. Shee, C.A. Thaiss, A. Reuben, J. Livny, R. Avraham, D.T. Frederick, M. Ligorio, K. Chatman, S.E. Johnston, C.M. Mosher, A. Brandis, G. Fuks, C. Gurbatri, V. Gopalakrishnan, M. Kim, M.W. Hurd, M. Katz, J. Fleming, A. Maitra, D.A. Smith, M. Skalak, J. Bu, M. Michaud, S.A. Trauger, I. Barshack, T. Golan, J. Sandbank, K.T. Flaherty, A. Mandinova, W.S. Garrett, S.P. Thayer, C.R. Ferrone, C. Huttenhower, S.N. Bhatia, D. Gevers, J.A. Wargo, T.R.

Golub, R. Straussman, Science, 357 (2017) 1156–1160. https://doi.org/10.1126/science.aah5043.

[9] P. Lehouritis, J. Cummins, M. Stanton, C.T. Murphy, F.O. McCarthy, G. Reid, C. Urbaniak, W.L. Byrne, M. Tangney, Sci. Reports 5 (2015) 14554. https://doi.org/10.1038/srep14554

[10] T.R. Zembower, in: V. Stosor, T.R. Zembower (Eds.), Infectious Complications in Cancer Patients, Springer International Publishing, Cham, 2014: pp. 43–89.

[11] L. Bacakova, M. Vandrovcova, I. Kopova, I. Jirka, Biomater. Sci. 6 (2018) 974–989. https://doi.org/10.1039/C8BM00028J

[12] G.T.M. Kadja, N.T.U. Culsum, R.M. Putri, Results Chem. 5 (2023) 100910. https://doi.org/10.1016/j.rechem.2023.100910

[13] J. Hao, I. Stavljenić Milašin, Z. Batu Eken, M. Mravak-Stipetic, K. Pavelić, F. Ozer, Molecules. 26 (2021) 6196. https://doi.org/10.3390/molecules26206196

[14] H.S. Sherry, in: S. M. Auerbach, K. A. Carrado, P. K. Dutta (Eds.), Handbook of Zeolite Science and Technology, Marcel Dekker, New York, 2003.

[15] C. Perego, A. Carati, in: J. Cejka, J. Paréz-Pariente, W.J. Roth, (Eds.), Zeolites: from model materials to industrial catalysts, Transworld Research Network, Trivandrum, 2008.

[16] R. Amorim, N. Vilaça, O. Martinho, R.M. Reis, M. Sardo, J. Rocha, A.M. Fonseca, F. Baltazar, I.C. Neves, J. Phys. Chem. C. 116 (2012) 25642–25650. https://doi.org/10.1021/jp3093868

[17] International Zeolite Association, Database of Zeolite Structures, News from the Structure Commission, http://www.iza-structure.org, (n.d.) (accessed May 2023); Zeolite Framework Types. http://asia.iza-structure.org/IZA-SC/ftc_table.php, (n.d.) (accessed in May 2023).

[18] M. Khodadadi Yazdi, P. Zarrintaj, H. Hosseiniamoli, A.H. Mashhadzadeh, M.R. Saeb, J.D. Ramsey, M.R. Ganjali, M. Mozafari, J. Mater. Chem. B. 8 (2020) 5992–6012. https://doi.org/10.1039/d0tb00719f

[19] P. Lalueza, M. Monzón, M. Arruebo, J. Santamaría, Mater. Res. Bull. 46 (2011) 2070–2076. https://doi.org/https://doi.org/10.1016/j.materresbull.2011.06.041

[20] L. Ferreira, C. Almeida-Aguiar, P. Parpot, A.M. Fonseca, I.C. Neves, RSC Adv. 5 (2015) 37188–37195. https://doi.org/10.1039/C5RA04960A

[21] R. Casañas Pimentel, E. San Martín Martínez, A. Monroy García, C. Gómez-García, Q.G. Alvarado Palacios, Bionanoscience. 3 (2013) 198–207. https://doi.org/10.1007/s12668-013-0085-6

[22] S. Gurunathan, M. Qasim, C. Park, H. Yoo, J.-H. Kim, K. Hong, Int. J. Mol. Sci. 19 (2018) 2269. https://doi.org/10.3390/ijms19082269

[23] P. Dutta, B. Wang, Coord. Chem. Rev. 383 (2019) 1–29. https://doi.org/10.1016/j.ccr.2018.12.014

[24] N. Vilaça, R. Amorim, A.F. Machado, P. Parpot, M.F.R. Pereira, M. Sardo, J. Rocha, A.M. Fonseca, I.C. Neves, F. Baltazar, Colloids Surfaces B Biointerfaces. 112 (2013) 237–244. https://doi.org/https://doi.org/10.1016/j.colsurfb.2013.07.042

[25] N. Vilaça, A.R. Bertão, E.A. Prasetyanto, S. Granja, M. Costa, R. Fernandes, F. Figueiredo, A.M. Fonseca, L. De Cola, F. Baltazar, I.C. Neves, Mater. Sci. Eng. C. 120 (2021) 111721. https://doi.org/10.1016/j.msec.2020.111721

[26] P. Noordhuis, U. Holwerda, C.L. Van der Wilt, C.J. Van Groeningen, K. Smid, S. Meijer, H.M. Pinedo, G.J. Peters, Ann. Oncol. 15 (2004) 1025–1032. https://doi.org/10.1093/annonc/mdh264

[27] S. Ghafouri-Fard, A. Abak, F.T. Anamag, H. Shoorei, F. Fattahi, S.A. Javadinia, A. Basiri, M. Taheri, Front. Oncol. 11 (2021) 658636. https://doi.org/10.3389/fonc.2021.658636

[28] P.R. Correia, Master Thesis, University of Minho, Braga, 2018. https://hdl.handle.net/1822/74124.

[29] L. Ferreira, J.F. Guedes, C. Almeida-Aguiar, A.M. Fonseca, I.C. Neves, Colloids Surfaces B Biointerfaces. 142 (2016) 141–147. https://doi.org/10.1016/j.colsurfb.2016.02.042

[30] C.-H. Chen, Y.-C. Lin, C.-F. Mao, W.-T. Liao, Res. Chem. Intermed. 45 (2019) 4463–4472. https://doi.org/10.1007/s11164-019-03842-z

[31] A.M. Fonseca, I.C. Neves, Microporous Mesoporous Mater. 181 (2013) 83–87. https://doi.org/10.1016/j.micromeso.2013.07.018

[32] A. Datt, E.A. Burns, N.A. Dhuna, S.C. Larsen, Microporous Mesoporous Mater. 167 (2013) 182–187. https://doi.org/10.1016/j.micromeso.2012.09.011

[33] M. Jeffroy, A. Boutin, A.H. Fuchs, J. Phys. Chem. B. 115 (2011) 15059–15066. https://doi.org/10.1021/jp209067n

[34] Y.M. Lee, S.J. Choi, Y. Kim, K. Seff, J. Phys. Chem. B. 109 (2005) 20137–20144. https://doi.org/10.1021/jp058185p

[35] J.B. Kaper, J.P. Nataro, H.L.T. Mobley, Nat. Rev. Microbiol. 2 (2004) 123–140. https://doi.org/10.1038/nrmicro818

[36] A. Perry, P. Lambert, Expert Rev. Anti. Infect. Ther. 9 (2011) 1149–1156. https://doi.org/10.1586/eri.11.137

[37] S.Y.C. Tong, J.S. Davis, E. Eichenberger, T.L. Holland, V.G. Fowler Jr., Clin. Microbiol. Rev. 28 (2015) 603–661. https://doi.org/10.1128/cmr.00134-14

[38] P. Costa, J.M. Sousa Lobo, Eur. J. Pharm. Sci. 13 (2001) 123–133. https://doi.org/10.1016/S0928-0987(01)00095-1

[39] S. Qin, W. Xiao, C. Zhou, Q. Pu, X. Deng, L. Lan, H. Liang, X. Song, M. Wu, Signal Transduct. Target. Ther. 7 (2022) 199. https://doi.org/10.1038/s41392-022-01056-1

[40] S.L. Clay, D. Fonseca-Pereira, W.S. Garrett, J. Clin. Invest. 132 (2022) e155101, https://doi.org/10.1172/JCI155101

[41] E. Hoste, E.N. Arwert, R. Lal, A.P. South, J.C. Salas-Alanis, D.F. Murrell, G. Donati, F.M. Watt, Nat. Commun. 6 (2015) 5932. https://doi.org/10.1038/ncomms6932

[42] N. Madhusudhan, M.R. Pausan, B. Halwachs, M. Durdević, M. Windisch, J. Kehrmann, V.K. Patra, P. Wolf, P. Boukamp, C. Moissl-Eichinger, L. Cerroni, J.C. Becker, G. Gorkiewicz, Cancers, 12 (2020) 541. https://doi.org/10.3390/cancers12030541

[43] Q. Huang, X. Wei, W. Li, Y. Ma, G. Chen, L. Zhao, Y. Jiang, S. Xie, Q. Chen, T. Chen, Cancers. 14 (2022) 5178. https://doi.org/10.3390/cancers14215178

[44] S. Davidsson, P. Mölling, J.R. Rider, M. Unemo, M.G. Karlsson, J. Carlsson, S.-O. Andersson, F. Elgh, B. Söderquist, O. Infect. Agent. Cancer. 11 (2016) 26. https://doi.org/10.1186/s13027-016-0074-9

[45] J.H. Gieringer, A.F. Wenz, H.M. Just, F.D. Daschner, Chemotherapy. 32 (1986) 418–424. https://doi.org/10.1159/000238445

[46] V. Singh, M. Brecik, R. Mukherjee, J.C. Evans, Z. Svetlíková, J. Blaško, S. Surade, J. Blackburn, D.F. Warner, K. Mikušová, V. Mizrahi, Chem. Biol. 22 (2015) 63–75. https://doi.org/10.1016/j.chembiol.2014.11.006

[47] C.A. 3rd Bodet, J.H. Jorgensen, D.J. Drutz, Antimicrob. Agents Chemother. 28 (1985) 437–439. https://doi.org/10.1128/AAC.28.3.437

[48] O. Martinho, P.J.G. Castro, R. Amorim, RSC Adv. 5 (2015) 29219–28227. https://doi.org/10.1039/C5RA03871E

[49] Á. Szegedi, M. Popova, I. Trendafilova, L. Trif, J. Mihály, J. Makk, V. Mavrodinova, Nano-Structures & Nano-Objects. 24 (2020) 100562. https://doi.org/https://doi.org/10.1016/j.nanoso.2020.100562.

[50] Y. Inoue, H. Hamashima, J. Biomater. Nanobiotechnol. 3 (2012) 114–117. http://dx.doi.org/10.4236/jbnb.2012.31015.

[51] R. Singh, C.S. Kumar, M. Banerjee, S. Gupta, ACS Appl. Bio Mater. 2 (2019) 5032–5041. https://doi.org/10.1021/acsabm.9b00724.

Journal Pre-proof

Highlights

- Dual Ag^{+}/5-FU@NaY (ZDS) as antimicrobial and antineoplastic agents;
- Higher amounts of Ag^{+} limit 5-FU drug loading into NaY in the dual system;
- ZDS outperformed individual drug effectiveness in inhibiting bacterial growth;
- ZDS has the potential to eliminate microbial infections in tumor-like microenvironments.

Journal Pre-proof

Journal Pre-proof

Declaration of interests

☒ The authors declare that they have no known competing financial interests or personal relationships that could have appeared to influence the work reported in this paper.

This manuscript is an original work; the results are novel and constitute an important contribution to the zeolite application as biomaterial. The manuscript has not been published previously and is not under consideration for publication elsewhere. The work was written by the stated authors who are all aware of its content and approve its submission.

All authors declare do not have a Conflict of Interest.

Journal Pre-proof